

# A Numerical Algorithm for Complex Biological Flow in Irregular Microdevice Geometries

D. Trebotich\*, P. Colella†, G. Miller‡, A. Nonaka‡, T. Marshall‡, S. Gulati†† and D. Liepmann††

\* Lawrence Livermore National Laboratory  
P.O. Box 808, L-560, Livermore, CA, USA, trebotich1@llnl.gov

† Lawrence Berkeley National Laboratory, Berkeley, CA, USA

‡ University of California, Davis, CA, USA

†† University of California, Berkeley, CA, USA

## ABSTRACT

We present a numerical algorithm to simulate non-Newtonian flow in complex microdevice components. The model consists of continuum viscoelastic incompressible flow in irregular microscale geometries. Our numerical approach is the projection method of Bell, Colella and Glaz (BCG) to impose the incompressibility constraint coupled with the polymeric stress splitting discretization of Trebotich, Colella and Miller (TCM). In this approach we exploit the hyperbolic structure of the equations of motion to achieve higher resolution in the presence of strong gradients and to gain an order of magnitude in the timestep. We also extend BCG and TCM to an embedded boundary method to treat irregular domain geometries which exist in microdevices. Our method allows for particle representation in a continuum uid. We present preliminary results for incompressible viscous flow with comparison to flow of DNA and simulants in microchannels and other components used in chem/bio microdevices.<sup>1</sup>

**Keywords:** non-Newtonian, viscoelasticity, Oldroyd-B, micro uidics, projection methods, embedded boundaries

## 1 INTRODUCTION

Micro Electro-Mechanical Systems (MEMS) technologies are at the forefront of engineering practice for the design of integrated uidic control and (bio)chemical sensing devices. Microscale uidic processors allow for portability, networking, low power and minimal reagent consumption and faster chemical reactions, but design/fab cycles are lengthy because trial-and-error design is time consuming. Advanced, high resolution models are needed to understand the fundamental physical processes of complex uids in these devices and to predict their behavior.

We consider incompressible flow of a viscoelastic uid at the microscale. Viscoelasticity is an appropriate model for particle-laden biological uids consisting of macromolecules (e.g., DNA, large proteins). The equations of

<sup>1</sup>This work was performed under the auspices of the U.S. Department of Energy by the University of California, Lawrence Livermore National Laboratory under contract No. W-7405-Eng-48.

motion are the incompressible Navier-Stokes equations and the Oldroyd-B polymeric stress equation:

$$\rho \mathbf{u}_t + \rho(\mathbf{u} \cdot \nabla) \mathbf{u} = -\nabla p + s \Delta \mathbf{u} + \nabla \cdot \boldsymbol{\tau} \quad (1)$$

$$\boldsymbol{\tau}_t + (\mathbf{u} \cdot \nabla) \boldsymbol{\tau} = \nabla \mathbf{u} \cdot \boldsymbol{\tau} + \boldsymbol{\tau} \cdot \nabla \mathbf{u}^T - \frac{1}{\lambda} (\boldsymbol{\tau} - 2 p \mathbf{D}(\mathbf{u})) \quad (2)$$

where  $\rho$  is the uid density,  $\mathbf{u}$  is the velocity of the uid,  $p$  is the isotropic pressure,  $\boldsymbol{\tau}$  is the shear stress, subscripts  $s$  and  $p$  refer to solvent and polymer, respectively, and  $\lambda$  is the relaxation time for the polymer. We note that continuum mechanics and applied mathematics conventions differ for the compact notation used in equations such as (2) where an upper-convected derivative exists. Here we use the convention  $(\nabla \mathbf{u})_{ij} = \frac{\partial u_i}{\partial x_j}$ .

A numerical approach to these equations of motion requires a formulation which is appropriate for constrained evolution equations. We choose the projection method, introduced by Chorin [1], made higher resolution by Bell, Colella, and Glaz (BCG) [2] and made suitably stable for highly elastic flows by Trebotich, Colella and Miller (TCM) [3]. We begin with the latter formulation and formally extend it to BCG by exploiting the hyperbolic nature of the equations. In doing so we gain the resolution of higher-order Godunov methods which are more robust than the Lax-Wendro method used in TCM; the methods also capture steep gradients while Lax-Wendro tends to smooth discontinuities as seen in compressible flow; and higher-order Godunov methods yield an order of magnitude increase in timestep over Lax-Wendro .

Microdevices consist of uidic components with complex geometries. We therefore extend the BCG and TCM methods to an embedded boundary formulation to treat irregular geometry. The embedded boundary (EB) method is a volume of uid method which takes a “cookie cutter” approach to irregular domain boundaries on Cartesian grids. Cut cells exist near boundaries and are treated with advanced discretization stencils [4][5], while the regular cells in the interior of the domain are discretized with known accurate and stable methods.

## 2 LINEAR ANALYSIS

In order to extend TCM to the higher-order Godunov methodology of BCG we must cast the stress equation in a hyperbolic, 1D homogeneous linear advection form:

$$\frac{\partial}{\partial t} W_\alpha + A_\alpha \frac{\partial}{\partial x_\alpha} W_\alpha = 0 \quad (3)$$

$$W_\alpha = (u_1, u_2, u_3, \alpha_1, \alpha_2, \alpha_3)^T \quad (4)$$

where the subscript  $\alpha$  indicates the direction. In [3] it was shown that the Oldroyd-B stress equation can be written in the following hyperbolic-elliptic form:

$$\begin{aligned} \frac{\partial \boldsymbol{\tau}}{\partial t} + \mathbf{u} \cdot \nabla \boldsymbol{\tau} - (\nabla \mathbf{u})(\boldsymbol{\tau} + a^2 \mathbf{I}) - (\boldsymbol{\tau} + a^2 \mathbf{I})(\nabla \mathbf{u})^T = \\ \frac{1}{\lambda} \boldsymbol{\tau} + \left[ \frac{\mu_p}{\lambda} \quad a^2 \right] [(\nabla \mathbf{u}) + (\nabla \mathbf{u})^T] \end{aligned} \quad (5)$$

where  $a^2$  is a wavespeed defined to capture both viscous ( $\lambda = 0$ ) and elastic ( $\lambda \rightarrow \infty$ ) limits of the Oldroyd-B equation (2).

We expand the left-hand side of equation (5) in 1D term by term and, coupled with the 1D homogeneous advection form of the Navier-Stokes equation (1), we obtain the following advection form of the equations of motion in the  $\alpha = 1$ , or  $x$ , direction:

$$A_1 = \begin{bmatrix} u_1 & 0 & 0 & \frac{1}{\rho} & 0 & 0 \\ 0 & u_1 & 0 & 0 & \frac{1}{\rho} & 0 \\ 0 & 0 & u_1 & 0 & 0 & \frac{1}{\rho} \\ 2\beta_1 & 0 & 0 & u_1 & 0 & 0 \\ 12 & \beta_1 & 0 & 0 & u_1 & 0 \\ 13 & 0 & \beta_1 & 0 & 0 & u_1 \end{bmatrix} \quad (6)$$

where  $\beta_1 = \alpha_{11} + a^2$ . In general,  $\beta_\alpha = \alpha_\alpha + a^2$ . The eigenvalues and corresponding eigenvectors are given in [3] with  $\mu_p/\lambda$  replaced by  $a^2$ .

## 3 VISCOELASTIC ALGORITHM

Our first goal is to design a high-resolution finite difference method on regular grids to evolve discrete velocity, pressure and stress in time for incompressible viscoelastic flow. At the beginning of each timestep,  $\Delta t$ , we know cell-centered grid representations at cell  $i$  of velocity, pressure and stress:  $\mathbf{u}_i^n$ ,  $\nabla p_i^{n-\frac{1}{2}}$ ,  $\boldsymbol{\tau}_i^n$ . The following is an algorithm to compute these quantities for discrete timesteps, i.e., to obtain the  $t = (n+1)\Delta t$  state,  $n = 0, 1, 2, \dots$

We use the predictor-corrector method of BCG in pressure form to evolve the discrete velocity field while enforcing the incompressibility constraint:

$$\begin{aligned} \mathbf{u}^* &= \mathbf{u}^n + \Delta t \left( [(\mathbf{u} \cdot \nabla) \mathbf{u}]^{n+\frac{1}{2}} + \frac{s}{\rho} \Delta \mathbf{u}^* \right. \\ &\quad \left. - \frac{1}{\rho} \nabla p_i^{n-\frac{1}{2}} + \frac{1}{\rho} \nabla \cdot \boldsymbol{\tau}_i^{n+\frac{1}{2}} \right) \end{aligned} \quad (7)$$

$$\mathbf{u}^{n+1} = \mathbf{u}^* - (\mathbf{I} - \mathbf{P})(\mathbf{u}^* + \frac{\Delta t}{\rho} \nabla p_i^{n-\frac{1}{2}}) \quad (8)$$

$$\nabla p_i^{n+\frac{1}{2}} = \frac{\rho}{\Delta t} (\mathbf{I} - \mathbf{P})(\mathbf{u}^* + \frac{\Delta t}{\rho} \nabla p_i^{n-\frac{1}{2}}) \quad (9)$$

where

$$\mathbf{Q} = \mathbf{G}\mathbf{L}^{-1}\mathbf{D} \quad (10)$$

$$\mathbf{P} = \mathbf{I} - \mathbf{Q} \quad (11)$$

$$\mathbf{L} = \mathbf{D}\mathbf{G} \quad (12)$$

and  $\mathbf{D}$  and  $\mathbf{G}$  are the discrete divergence and gradient operators, respectively. For now we choose the backward Euler method to discretize the viscous term in time in equation (7).

In order to construct the solution,  $W_i^{n+\frac{1}{2}} = (u_1, u_2, u_3, \alpha_{11}, \alpha_{12}, \alpha_{13})^{T,n+\frac{1}{2}}$ , for a given direction  $\alpha = 1$ , we use characteristic tracing of the variables. We perform a Taylor expansion in 1D from the solution  $W_i^n$  at cell centers,  $i$ , to plus and minus edges of the cell and the half time, using the PDE (3) to eliminate the temporal derivative:

$$\hat{W}_{i,\pm}^{n+\frac{1}{2}} = W_i^n + \frac{1}{2} (\pm I - \frac{\Delta t}{\Delta x} A_1) P^\pm (\Delta_1 W_i^n) + \frac{\Delta t}{2} S_1. \quad (13)$$

where

$$P^\pm(W) = \sum_{\pm \Lambda_k > 0} (l_k \cdot W) r_k \quad (14)$$

is the eigenvalue decomposition, summed over characteristics, and  $r_k$  and  $\Lambda_k$  are the right eigenvectors and corresponding eigenvalues of the matrix  $A_i$ , and  $l_k$  are the left eigenvectors. Here the source term,  $S_1$ , has been added to the right-hand side of equation (3) but does not include the lagged pressure gradient,  $\nabla p_i^{n-\frac{1}{2}}$ . As a result of extrapolation to edges a Riemann problem exists at each edge with solution

$$\tilde{W}_{i+\frac{1}{2}} = W_{i,+} + \sum_{\Lambda_k < 0} [l_k \cdot (W_{i+1,-} - W_{i,+}) r_k]. \quad (15)$$

The time-centered velocities are then corrected to account for the pressure gradient:

$$\mathbf{u}^{n+\frac{1}{2}} = \tilde{\mathbf{u}} - (\mathbf{I} - \mathbf{P}^{mac})(\tilde{\mathbf{u}}) \quad (16)$$

from which the convective derivative,  $(\mathbf{u} \cdot \nabla) \mathbf{u}^{n+\frac{1}{2}}$ , can be computed. A predicted velocity that is not necessarily divergence-free is obtained from (7) and projected to obtain  $\mathbf{u}^{n+1}$ . The stress is then updated to the new time:

$$\begin{aligned} \boldsymbol{\tau}^{n+1} &= \boldsymbol{\tau}^n + \Delta t \left( (\mathbf{u} \cdot \nabla) \boldsymbol{\tau} \right. \\ &\quad \left. + \nabla \mathbf{u} \cdot (\boldsymbol{\tau} + a^2 \mathbf{I}) + (\boldsymbol{\tau} + a^2 \mathbf{I}) \cdot \nabla \mathbf{u}^T \right)^{n+\frac{1}{2}} \\ &\quad - \frac{\Delta t}{\lambda} (\boldsymbol{\tau}^{n+1} - 2 \mathbf{P}(\mathbf{u}^{n+1})). \end{aligned} \quad (17)$$

The algorithm is subject to the following stability restriction on the timestep:

$$\max_i [|u_1| + (2(\alpha_{11} + a^2)/\rho)^{\frac{1}{2}}] \Delta t < \sigma \Delta x \quad (18)$$

with  $\sigma < 1$ .

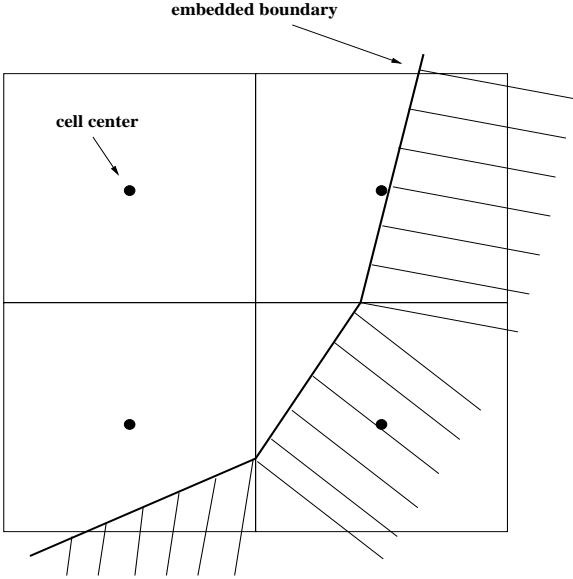


Figure 1: Example of embedded boundary “cutting” regular cells.

#### 4 IRREGULAR GEOMETRY

The second goal of this paper is to compute flows in the complex geometries which occur in microfluidic devices. We do this by extending BCG to embedded boundaries. The embedded boundary method is an approach in which regular cells on a Cartesian grid are cut by physical boundaries and/or interfaces (see Figure 1). Higher-order stencils are constructed near boundaries where irregular, or “cut”, cells occur while discretizations with known accuracy and stability requirements are employed on the interior regular cells [4], [5]. We make use of the Chombo software libraries [6], [7] which provide a framework for data management, numerical operators and linear solvers needed in an EB formulation. We adapt the Chombo framework to incompressible flow by developing the fundamental numerical operators with relevant features—namely, viscous (Dirichlet) boundary conditions.

#### 5 RESULTS

We apply our method to flow of a DNA solution in 2D and 3D contraction microchannels. Experimental data has been used to obtain the rheological parameters specific to this fluid and to also validate the computational model [8]:  $\rho = 1 \text{ g/ml}$ ,  $\lambda = 1.14 \text{ s}$ ,  $\eta_s = .2538 \text{ g/cm/s}$  and  $\eta_p = .02688 \text{ g/cm/s}$ . The experimental flow rate is  $30 \mu\text{l/hr}$ .

Figures 2 and 3 show the experimental channel and velocity profile results obtained using Digital Particle Image Velocimetry (DPIV). We compare the experimental results with computations of a flow in a similar channel. Figure 4 shows calculated viscoelastic flow in a 3D

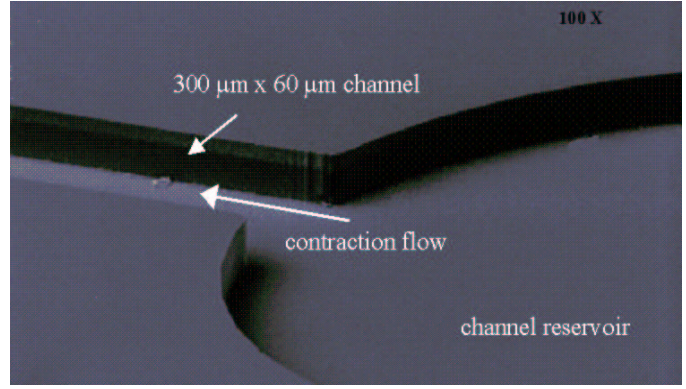


Figure 2: Experimental contraction channel (*Shrewsbury*).

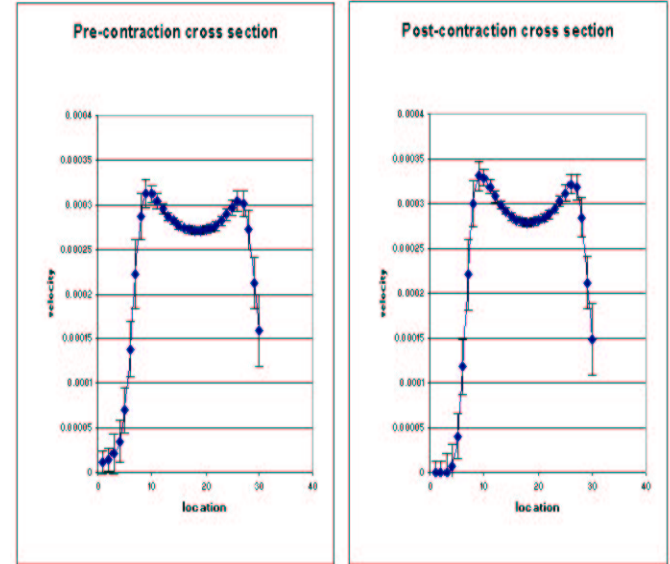


Figure 3: Experimental velocity profiles just before and after contraction in m/sec (*Gulati*).

contraction duct and demonstrates the same character in the profile—a dip, or top-hat. As for the magnitudes we note a difference in scaling—experimental data are in m/s, computations are in cm/s. Also, the experimental flow rate is based on average velocity through the contraction, as if the contraction were the inlet. For computations, the same average velocity is applied at the inlet of the large section of the channel. Despite the discrepancy, we find that the magnitudes are within the error bars of the experiments. Finally, Figures 5 and 6 depict viscous flow in irregular geometry, approximating the experimental device, and demonstrating our embedded boundary capability. These results are obtained from 2D simulations where the top-hat profile does not exist as it is a 3D phenomenon.

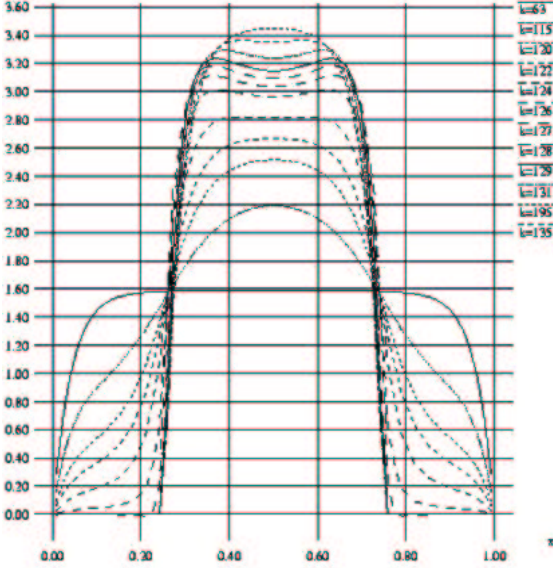


Figure 4: Series of computed velocity profiles for viscoelastic flow through 3D contraction microchannel.

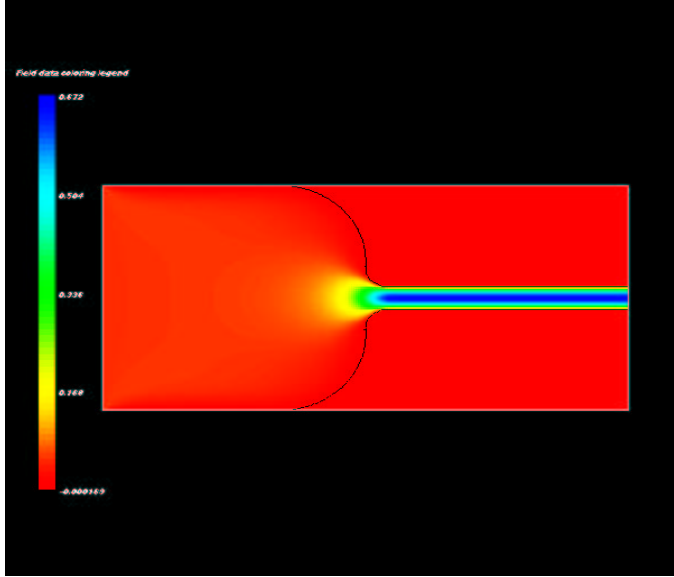


Figure 5: Velocity data for viscous flow in a 2D contraction channel with irregular boundaries.

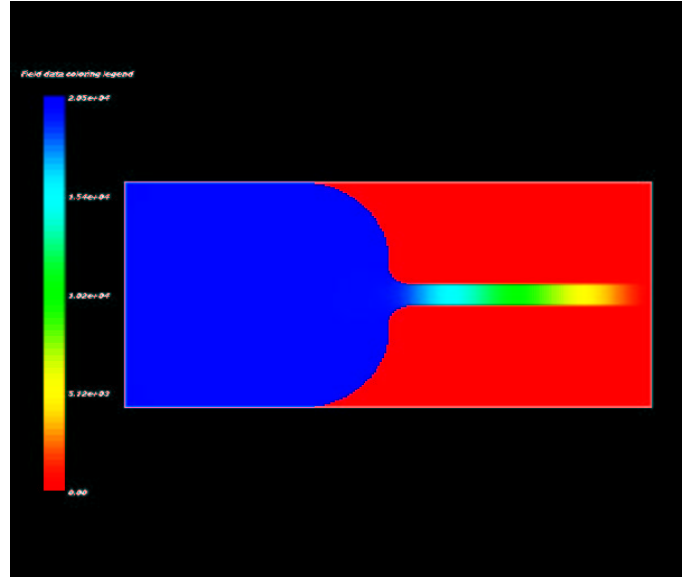


Figure 6: Pressure for viscous flow in a 2D contraction channel with irregular boundaries.

## 6 CONCLUSION

We demonstrate a high resolution computational capability which models non-Newtonian, viscoelastic flow in irregular geometries. The numerical model compares well with experimental results for flow of a DNA solution in a bioMEMS device. This work provides the foundation for computing uid flows in more complicated microdevice components as well as biological systems. In addition to the continuum model we also allow for a particle representation in the bulk uid.

## REFERENCES

- [1] Chorin, A. J., *Math. Comp.*, **22**, 745-762, 1968.
- [2] J. B. Bell, P. Colella and H. M. Glaz, *J. Comp. Phys.*, **85**, 257-283, 1989.
- [3] D. Trebotich, P. Colella and G. H. Miller, *J. Comp. Phys.*, submitted.
- [4] H. Johansen and P. Colella, *J. Comp. Phys.*, **147**, 60-85, 1998.
- [5] P. McCorquodale, P. Colella and H. Johansen, *J. Comp. Phys.*, **173**, 620-635, 2001.
- [6] P. Colella, D. T. Graves, T. J. Ligocki, D. F. Martin, D. Modiano, D. B. Sera ni and B. Van Straalen, Chombo Software Package for AMR Applications, unpublished, 2000.
- [7] P. Colella, D. T. Graves, T. J. Ligocki, D. Modiano and B. Van Straalen, EBChombo Software Package for Cartesian Grid, Embedded Boundary Applications, unpublished, 2000.
- [8] P. Shrewsbury, S. J. Muller and D. Liepmann, *Biomedical Microdevices*, **3**, 225-238, 2001.